Article

Synthesis of Ordered Mesoporous NiO with Crystalline Walls and a Bimodal Pore Size Distribution

Feng Jiao, Adrian H. Hill, Andrew Harrison, Aaron Berko, Alan V. Chadwick, and Peter G. Bruce

J. Am. Chem. Soc., **2008**, 130 (15), 5262-5266 • DOI: 10.1021/ja710849r • Publication Date (Web): 19 March 2008

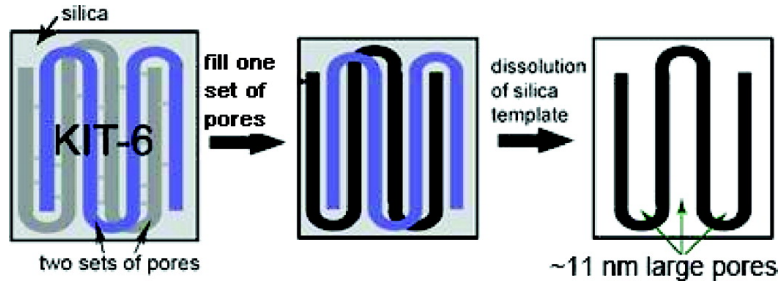

More About This Article

Additional resources and features associated with this article are available within the HTML version:

- Supporting Information
- Links to the 3 articles that cite this article, as of the time of this article download
- Access to high resolution figures
- Links to articles and content related to this article
- Copyright permission to reproduce figures and/or text from this article

View the Full Text HTML

J|A|C|S
ARTICLES

Published on Web 03/19/2008

Synthesis of Ordered Mesoporous NiO with Crystalline Walls and a Bimodal Pore Size Distribution

Feng Jiao,[†] Adrian H. Hill,[‡] Andrew Harrison,[‡,§] Aaron Berko,[¶] Alan V. Chadwick,[¶] and Peter G. Bruce*[,†]

EaStChem and School of Chemistry, University of St. Andrews, St. Andrews, Fife KY16 9ST, U.K., EaStChem and School of Chemistry, University of Edinburgh, Joseph Black Building, West Mains Road, Edinburgh EH9 3JJ, U.K., Institut Laue-Langevin 6, rue Jules Horowitz, BP 156-38042 Grenoble Cedex 9, France, and Centre for Materials Research, School of Physical Sciences, University of Kent, Canterbury, Kent CT2 7NR, U.K.

Received December 5, 2007; E-mail: p.g.bruce@st-andrews.ac.uk

Abstract: A mesoporous solid with crystalline walls and an ordered pore structure exhibiting a bimodal pore size distribution (3.3 and 11 nm diameter pores) has been synthesized. Previous attempts to synthesize solids with large ordered mesopores by hard templating focused on the preparation of templates with thick walls (the thick walls become the pores in the target materials), something that has proved difficult to achieve. Here the large pores (11 nm) do not depend on the synthesis of a template with thick walls but instead on controlling the microporous bridging between the two sets of mesopores in the KIT-6 template. Such control determines the relative proportion of the two pore sizes. The wall thickness of the 3D cubic NiO mesopore has also been varied. Preliminary magnetic characterization indicates the freezing of uncompensated moments or blocking of superparamagnetism.

Introduction

Interest in mesoporous solids (pore size 2–50 nm) has become intense in recent years.[1–9] The advent of hard templating, where one mesoporous solid (often a mesoporous silica) is used as a template within which to grow another mesoporous solid (e.g., a transition metal oxide), has proved a powerful tool with which to synthesize a wide range of mesoporous materials combining an ordered pore structure and crystalline walls.[10–14] However, the method, as originally exploited, has its limitations. For example, it can be challenging to synthesize mesopores exhibiting mixed valency or with oxidation states that are difficult to stabilize in solution or that contain Li.[15,16] Previously, we reported the synthesis of the mesoporous spinel Fe_3O_4 and lithium containing compound $LiCoO_2$ by post-template redox reaction and post-template reaction with a lithium source, respectively, thus demonstrating access to a wider range of mesoporous solids.[16–18]

Another limitation is the pore sizes that may be obtained for mesoporous solids with an ordered pore structure and crystalline walls.[7,10,11,19,20] Silica xerogels or carbon aerogels have been used as hard templates to produce inorganic solids with a pore size up to 18 nm, but the pores are disordered.[20–22] To obtain ordered mesoporous oxides with crystalline walls, mesoporous silicas with an ordered pore structure, such as SBA-15, SBA-16, and KIT-6, are used as hard templates, but such a route limits the pore size to less than 7 nm.[16,23–30] Efforts to prepare large and ordered porous solids by hard templating have focused

[†] University of St. Andrews.
[‡] University of Edinburgh.
[§] Institut Laue-Langevin 6.
[¶] University of Kent.

(1) Kresge, C. T.; Leonowicz, M. E.; Roth, W. J.; Vartuli, J. C.; Beck, J. S. *Nature* **1992**, *359*, 710.
(2) Huo, Q. S.; Margolese, D. I.; Stucky, G. D. *Chem. Mater.* **1996**, *8*, 1147.
(3) Sayari, A. *Chem. Mater.* **1996**, *8*, 1840.
(4) Corma, A. *Chem. Rev.* **1997**, *97*, 2373.
(5) Yang, P. D.; Zhao, D. Y.; Margolese, D. I.; Chmelka, B. F.; Stucky, G. D. *Nature* **1998**, *396*, 152.
(6) Ying, J. Y.; Mehnert, C. P.; Wong, M. S. *Angew. Chem., Int. Ed.* **1999**, *38*, 56.
(7) Schuth, F. *Chem. Mater.* **2001**, *13*, 3184.
(8) Davis, M. E. *Nature* **2002**, *417*, 813.
(9) Antonietti, M.; Ozin, G. A. *Chem.—Eur. J.* **2004**, *10*, 29.
(10) Yang, H. F.; Zhao, D. Y. *J. Mater. Chem.* **2005**, *15*, 1217.
(11) Lu, A. H.; Schuth, F. *Adv. Mater.* **2006**, *18*, 1793.
(12) Joo, S. H.; Choi, S. J.; Oh, I.; Kwak, J.; Liu, Z.; Terasaki, O.; Ryoo, R. *Nature* **2001**, *412*, 169.
(13) Kleitz, F.; Choi, S. H.; Ryoo, R. *Chem. Commun.* **2003**, 2136.
(14) Ryoo, R.; Joo, S. H.; Kruk, M.; Jaroniec, M. *Adv. Mater.* **2001**, *13*, 677.
(15) Brezesinski, T.; Groenewolt, M.; Antonietti, M.; Smarsly, B. *Angew. Chem., Int. Ed.* **2006**, *45*, 781.
(16) Jiao, F.; Shaju, K. M.; Bruce, P. G. *Angew. Chem., Int. Ed.* **2005**, *44*, 6550.
(17) Jiao, F.; Jumas, J. C.; Womes, M.; Chadwick, A. V.; Harrison, A.; Bruce, P. G. *J. Am. Chem. Soc.* **2006**, *128*, 12905.
(18) Jiao, F.; Harrison, A.; Hill, A. H.; Bruce, P. G. *Adv. Mater.* **2007**, *19*, 4063.
(19) Valdes-Solis, T.; Fuertes, A. B. *Mater. Res. Bull.* **2006**, *41*, 2187.
(20) Fuertes, A. B. *J. Phys. Chem. Solids* **2005**, *66*, 741.
(21) Li, W. C.; Lu, A. H.; Weidenthaler, C.; Schuth, F. *Chem. Mater.* **2004**, *16*, 5676.
(22) Li, W. C.; Lu, A. H.; Schmidt, W.; Schuth, F. *Chem.—Eur. J.* **2005**, *11*, 1658.
(23) Yue, W. B.; Zhou, W. Z. *J. Mater. Chem.* **2007**, *17*, 4947.
(24) Wang, Y. Q.; Yang, C. M.; Schmidt, W.; Spliethoff, B.; Bill, E.; Schuth, F. *Adv. Mater.* **2005**, *17*, 53.
(25) Tian, B. Z.; Liu, X. Y.; Solovyov, L. A.; Liu, Z.; Yang, H. F.; Zhang, Z. D.; Xie, S. H.; Zhang, F. Q.; Tu, B.; Yu, C. Z.; Terasaki, O.; Zhao, D. Y. *J. Am. Chem. Soc.* **2004**, *126*, 865.

 10.1021/ja710849r CCC: $40.75

on the synthesis of ordered porous templates with thick walls (the walls of the template become the pores of the target mesoporous materials). Such synthesis has proved difficult.[10,11]

Here we show that it is possible to produce an ordered mesoporous solid with crystalline walls, specifically NiO, and with a pore diameter up to 11 nm. The resulting mesoporous NiO exhibits a bimodal pore size distribution (3.3 and 11 nm diameter). A bimodal pore size distribution has been observed previously using hard template routes and explained by insufficient impregnation of the precursor or infiltration of the precursor in the space between the particles of the template.[22,27,31,32] In this paper, we demonstrate, for the first time, that by disconnecting the two sets of mesopores in the KIT-6 template a bimodal pore size distribution may be generated and the proportion of the two sizes (3.3 and 11 nm) may be varied by controlling the temperature of the hydrothermal reaction used to form the KIT-6 silica template. Furthermore, this is the first example of a 3D mesoporous NiO with a cubic mesoporous symmetry.

Experimental Procedures

Preparation of the mesoporous silica, KIT-6, has been reported previously.[13,33] A typical synthesis procedure was as follows: 10 g of poly(ethylene glycol)−block−poly(propylene glycol)−block−poly(ethylene glycol) P123 (average $M_n \sim 5800$, Aldrich) was mixed with 282.5 mL of water and 16.75 mL of concentrated HCl (37 wt %, Fisher) in a beaker. The mixture was stirred at 35 °C until a homogeneous solution was obtained. Then, 10 g of *n*-butanol (99.4+%, Aldrich) was added, and this mixture was stirred for 1 h before 21.5 g of tetraethyl orthosilicate (TEOS, 98%, Aldrich) was added. After stirring at 35 °C for 24 h, the mixture was transferred into autoclaves which were sealed and maintained at three different temperatures, 80, 100, and 130 °C, for another 24 h. The resulting mixtures were filtered and dried at 60 °C, then added to 300–400 mL of ethanol and 20–30 mL of concentrated HCl (37 wt %, Fisher) in an 800 mL beaker. After stirring at room temperature for 1–2 h, the mixture was filtered and washed with water and ethanol several times. The final sample was dried at 60 °C and calcined at 500 °C for 3 h under air to remove the polymer template. The resulting three mesoporous silicas (KIT-6) were characterized by N_2 adsorption and transmission electron microscopy (TEM) analysis before being used as a hard template in the following procedure.

A typical synthesis of mesoporous NiO was as follows: 4 g of $Ni(NO_3)_2 \cdot 6H_2O$ (96%, Aldrich) was dissolved in 150 mL of ethanol, followed by addition of 5 g of mesoporous silica KIT-6. After stirring at room temperature in a fume cupboard until all the solution had been absorbed, the powder was redispersed in 100 mL of dry *n*-hexane under stirring in an open beaker. After all the solvent had evaporated, the sample was heated slowly to 550 °C and calcined at that temperature for 3 h. The resulting sample was treated twice with a hot aqueous solution of 2 M NaOH to remove the silica template, followed by washing with water several times and then drying at 60 °C. Mesoporous NiO prepared by using KIT-6 at 80, 100, and 130 °C was denoted as NiO-80, NiO-100, and NiO-130, respectively.

TEM studies were carried out by using a JEOL JEM-2011. This TEM uses a LaB6 filament as the electron source, and the accelerate voltage is 200 keV. TEM and HRTEM images were both recorded by a Gatan CCD camera in a digital format. Wide-angle powder X-ray diffraction data were collected in a Stoe STADI/P powder diffractometer operating in transmission mode and with a low-angle position-sensitive detector. Incident radiation was generated using a Fe $K\alpha_1$ source ($\lambda = 1.936$ Å). Low-angle powder X-ray diffraction data were collected using a Rigaku/MSC, D/max-rB with Cu $K\alpha_1$ radiation ($\lambda = 1.541$ Å) operating in reflection mode and a scintillation detector. N_2 adsorption−desorption analysis was carried out using a Micromeritics ASAP 2020. The typical sample weight used in the measurement was 100–200 mg. The outgas condition was set to 180 min at 120 °C under vacuum, and all adsorption−desorption measurements were carried out under liquid nitrogen temperature. Oxidation states were verified by XANES, and local structure was probed by EXAFS on Station 9.3 at the CCLRC Daresbury Laboratory SRS, U.K. The magnetic measurements were taken using a MPMS Quantum Design SQUID magnetometer. Weighed samples were encapsulated in gelatin and then placed in a diamagnetic straw, attached to the sample holder, which was connected to the SQUID system. Data were collected in an applied field of 0.01 T, first after cooling from 320 to 1.8 K in zero field (zfc) and then after cooling through the same temperature range in a field of 0.01 T (fc).

Results and Discussion

In order to produce a material with a highly ordered mesoporous structure throughout, it is essential to achieve a high degree of infiltration and wetting of the precursor solution within the pore structure of the hard template KIT-6. This was achieved in the case of mesoporous NiO by infiltrating a solution of $Ni(NO_3)_2$ in ethanol rather than water and by redispersing in hexane. In this way, it was possible to achieve a very high degree of pore filling.

The three 3D mesoporous NiO materials were examined by transmission electron microscopy (TEM). All three samples show a highly ordered pore structure (Figure 1). By examining many particles, it has been demonstrated that this highly ordered mesoporous structure is present throughout each material, confirming the high level of infiltration achieved by the solution precursor. The symmetry of the mesostructure for NiO-80, NiO-100, and NiO-130 is that of the 3D template KIT-6, *Ia*3*d*. The cubic lattice parameters, a_0, extracted from the TEM data are 213, 230, and 258 Å for NiO-80, NiO-100, and NiO-130, respectively. The wall thicknesses for NiO-80, NiO-100, and NiO-130 estimated from TEM results are 5.5, 6.8, and 7.8 nm, respectively. These values are in good agreement with the pore sizes of the corresponding mesoporous silica templates, which are 5.3, 7.1, and 8.0 nm (Table 1), respectively (the pores of the template become the walls of the mesoporous NiO materials).[13,33] The NiO particles are of typical diameter, 0.2–0.5 μm, and are approximately spherical, consistent with a 3D process of nucleation and growth within the isotropic pore structure of the KIT-6 template.

The pore structures of mesoporous NiO were examined by N_2 adsorption−desorption measurements, the results of which are presented in Figure 2 and summarized in Table 1. The isotherms with H1 hysteresis loops, observed for all three mesoporous NiO (Figure 2a), are similar in shape to those observed previously for many other mesoporous transition metal

(26) Shen, W. H.; Dong, X. P.; Zhu, Y. F.; Chen, H. R.; Shi, J. L. *Microporous Mesoporous Mater.* **2005**, *85*, 157.
(27) Jiao, K.; Zhang, B.; Yue, B.; Ren, Y.; Liu, S. X.; Yan, S. R.; Dickinson, C.; Zhou, W. Z.; He, H. Y. *Chem. Commun.* **2005**, 5618.
(28) Jiao, F.; Bruce, P. G. *Adv. Mater.* **2007**, *19*, 657.
(29) Tian, B. Z.; Liu, X. Y.; Yang, H. F.; Xie, S. H.; Yu, C. Z.; Tu, B.; Zhao, D. Y. *Adv. Mater.* **2003**, *15*, 1370.
(30) Salabas, E. L.; Rumplecker, A.; Kleitz, F.; Radu, F.; Schuth, F. *Nano Lett.* **2006**, *6*, 2977.
(31) Shi, Y. F.; Meng, Y.; Chen, D. H.; Cheng, S. J.; Chen, P.; Yang, T. F.; Wan, Y.; Zhao, D. Y. *Adv. Funct. Mater.* **2006**, *16*, 561.
(32) Zhou, L.; Li, H. Q.; Yu, C. Z.; Zhou, X. F.; Tang, J. W.; Meng, Y.; Xia, Y. Y.; Zhao, D. Y. *Carbon* **2006**, *44*, 1601.
(33) Kim, T. W.; Kleitz, F.; Paul, B.; Ryoo, R. *J. Am. Chem. Soc.* **2005**, *127*, 7601.

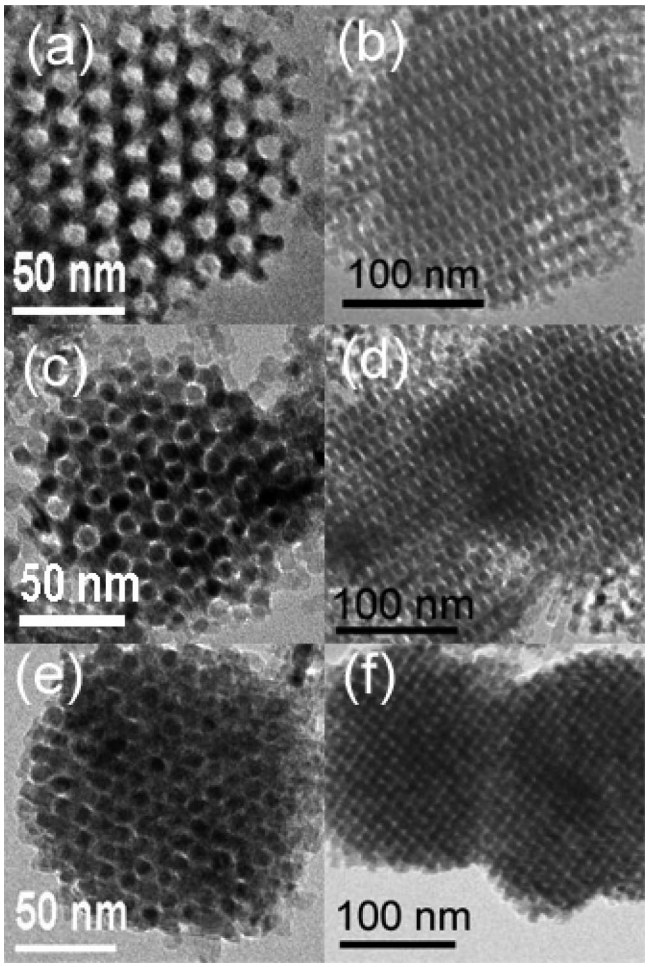

Figure 1. TEM images for mesoporous (a, b) NiO-80, (c, d) NiO-100, and (e, f) NiO-130 recorded along different directions.

Table 1. Summary of BET Surface Areas, Pore Diameters, and Wall Thicknesses for KIT-6 Synthesized Hydrothermally at 80, 100, and 130 °C (Denoted as KIT-6-80, KIT-6-100, and KIT-6-130, Respectively) and Corresponding Mesoporous NiO Replicas

	BET surface area (m^2/g)	pore diameter[a] (nm)	wall thickness[b] (nm)
KIT-6-80	820	5.3	3.6
KIT-6-100	816	7.1	3.4
KIT-6-130	787	8	3.3
NiO-80	108.6	3.1/11.1/31	5.5
NiO-100	94.1	3.15/11.3/33	6.8
NiO-130	81.8	3.3/29	7.8

[a] The pore size distribution is calculated from the desorption isotherm by the BJH method. [b] The wall thickness is estimated by TEM analysis.

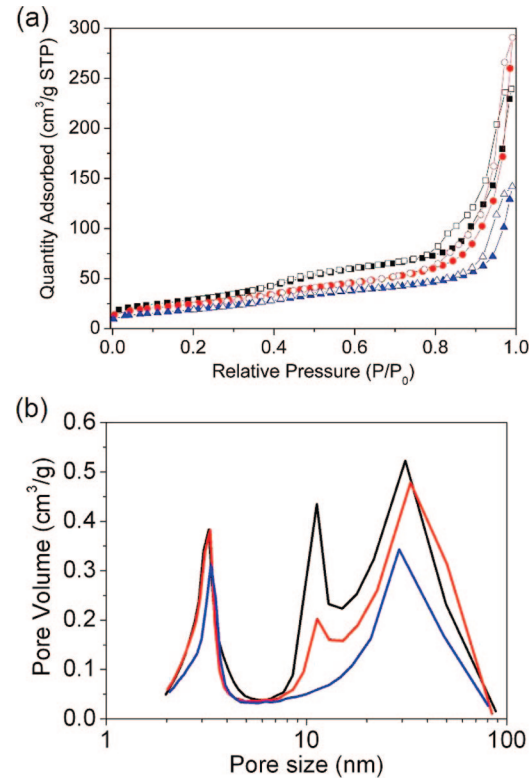

Figure 2. (a) N_2 adsorption−desorption isotherms for NiO-80 (black), NiO-100 (red), and NiO-130 (blue). (b) Pore size distributions calculated from desorption isotherms by the BJH method for NiO-80 (black), NiO-100 (red), and NiO-130 (blue).

Scheme 1. Mechanism By Which Two Pore Sizes in Mesoporous NiO Can Occur

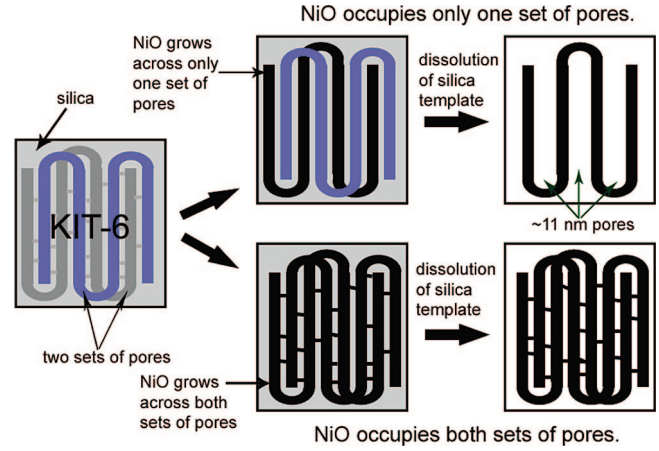

oxides synthesized by the hard template route.[24,27,28,34] The pore size distributions calculated from the desorption isotherms by the BJH method are shown as a plot of the relative pore filling versus pore size in Figure 2b. The first peak at 3.1, 3.15, and 3.3 nm for NiO-80, NiO-100, and NiO-130, respectively, is in agreement with the wall thickness (~3.3 nm) of KIT-6 (see Table 1). For NiO-80 and NiO-100, but not NiO-130, there is also a peak at 11 nm; that is, NiO-80 and NiO-100 exhibit a bimodal pore size distribution. The TEM image of this large pore is shown in Figure 1a.

KIT-6 is composed of two sets of interpenetrating mesopores. Whereas early reports indicated that each set of mesopores was independent, recent studies have contradicted this view, suggesting that they are interconnected by micropores, as in SBA-15.[33,35] If NiO growing within the pores of KIT-6 can do so across both sets of pores, then the resulting mesoporous NiO will have a wall thickness equivalent to the size of the KIT-6 mesopores (5–8 nm) and a pore diameter equivalent to the KIT-6 wall thickness (~3.3 nm). If, on the other hand, NiO grows within only one set of the KIT-6 mesopores, then the resulting

(34) Zhu, K. K.; Yue, B.; Zhou, W. Z.; He, H. Y. *Chem. Commun.* **2003**, 98.

(35) Sakamoto, Y.; Kim, T. W.; Ryoo, R.; Terasaki, O. *Angew. Chem., Int. Ed.* **2004**, *43*, 5231.

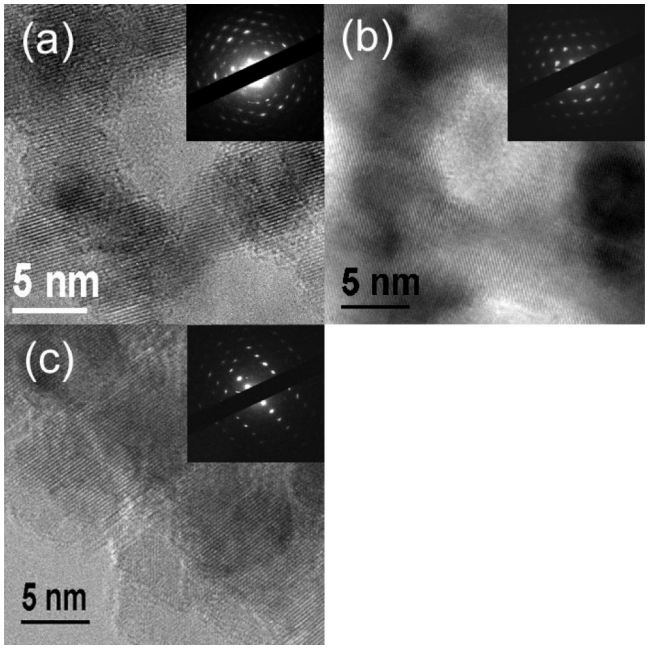

Figure 3. HRTEM images and selected area electron diffractions (insets) for (a) NiO-80, (b) NiO-100, and (c) NiO-130.

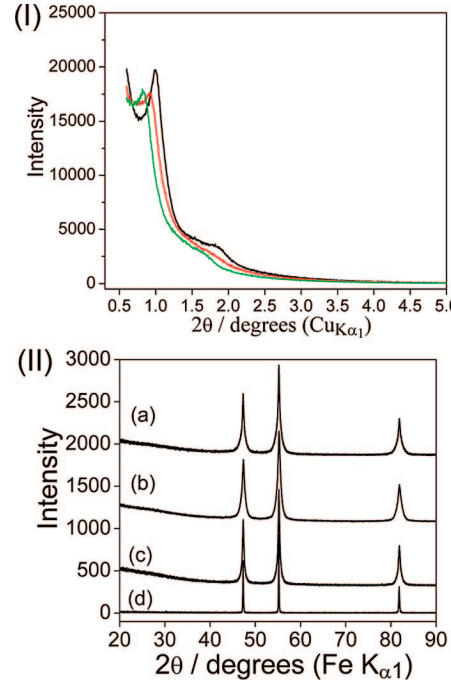

Figure 4. (I) Low-angle PXRD patterns for NiO-80 (black line), NiO-100 (red line), and NiO-130 (green line). (II) Powder X-ray diffraction patterns for (a) NiO-80, (b) NiO-100, (c) NiO-130, and (d) bulk NiO.

mesoporous NiO will still have a wall thickness of 5–8 nm but the pore diameter will be greater than before (~11 nm), equivalent to the dimensions of two walls plus a pore of KIT-6 (Scheme 1).

The differences observed in the mesostructures for the three NiO materials reflect the differences in the connectivity between the two sets of mesopores in KIT-6. For NiO-130, mesoporous NiO must grow across both sets of the mesopores in KIT-6 since only ~3.3 nm pores are observed in NiO; that is, the two sets of mesopores in KIT-6 must be connected by micropores. Examination of HRTEM images for NiO-130 shows coherence of the lattice fringes throughout the particles, and selected area electron diffraction on a single particle indicates a single-crystal-like structure, consistent with structural coherence across the two sets of pores (Figure 3c). For KIT-6 synthesized below 130 °C, the micropores must be less well developed, leading to less connectivity between the two sets of mesopores and hence the appearance of the 11 nm pores in NiO-80 and NiO-100. Figure 3a,b shows that there is structural coherence across the particles for NiO-80 and NiO-100. The relative intensities of the peaks in Figure 2b corresponding to the 3.3 and 11 nm pores differ between NiO-80 and NiO-100, demonstrating a difference in the proportions of the two pore sizes. The proportion of the 11 nm pores decreases with increasing temperature, and the 11 nm pores disappear entirely for NiO-130. These results are consistent with the change in the microporous connectivity of KIT-6 achieved by changing the temperature used to prepare the template.[33] The results show that it is possible to control the appearance and proportion of large (11 nm) pores in 3D mesoporous NiO by varying the KIT-6 synthesis temperature. The BET surface areas for NiO-80, NiO-100, and NiO-130, calculated from the sorption data, are 108.6, 94.1, and 81.8 $m^2 g^{-1}$ (Table 1) and are similar to the surface areas of other mesoporous transition metal oxides templated by KIT-6.[17,26,27,36,37]

The results described above were obtained at a $Ni(NO_3)_2$ to KIT-6 weight ratio of 0.8 and a calcination temperature of 550 °C. The effect of varying the impregnation ratio, $Ni(NO_3)_2$ to KIT-6, and the calcination temperature on the bimodal pore size distribution has also been investigated. The $Ni(NO_3)_2$/KIT-6 weight ratio was varied from 0.5 to 2. For NiO-80 and NiO-100, there is a slight increase in the ratio of 11 to 3.3 nm pores at low $Ni(NO_3)_2$/KIT-6 weight ratios, while there is a small decrease in the ratio of 11 to 3.3 nm pores when more $Ni(NO_3)_2$ is added. In the case of NiO-130, no significant change was observed. These results indicate that, although previous studies suggested that insufficient impregnation of the precursor may result in a bimodal pore size distribution, this is not observed in the present study.[32] The influence of varying the calcination temperature was also examined. A sample was heated at different temperatures from 400 to 800 °C, but no significant change in the pore size distribution of NiO was observed.

The 3D mesoporous NiO samples were examined by low-angle powder X-ray diffraction (Figure 4I). The data show one sharp peak at 0.8–1.0° and another broad peak at 1.5–1.8° (Cu $K\alpha_1$). These peaks may be indexed as the (211) and (332) reflections of the cubic unit cell with lattice parameters of a_0 = 216, 236, and 263 Å for NiO-80, NiO-100, and NiO-130, respectively, consistent with the a_0 values obtained from the TEM data.

Wide-angle powder X-ray diffraction data for mesoporous NiO are shown in Figure 4II, where they are compared with data for bulk NiO. The peaks of all phases are coincident, demonstrating that the simple cubic rock salt structure ($Fm\bar{3}m$) dominates the walls of the mesoporous solid.

The three mesoporous NiO materials were examined by XANES/EXAFS and compared with bulk NiO (99% pure, Aldrich, color green); see Figure S1 in Supporting Information. The XANES data demonstrate that the oxidation state is Ni^{2+} in all the samples. The EXAFS data for mesoporous and bulk NiO are shown in Figure S2. The agreement between the major

(36) Jiao, F.; Harrison, A.; Jumas, J. C.; Chadwick, A. V.; Kockelmann, W.; Bruce, P. G. *J. Am. Chem. Soc.* **2006**, *128*, 5468.
(37) Laha, S. C.; Ryoo, R. *Chem. Commun.* **2003**, 2138.

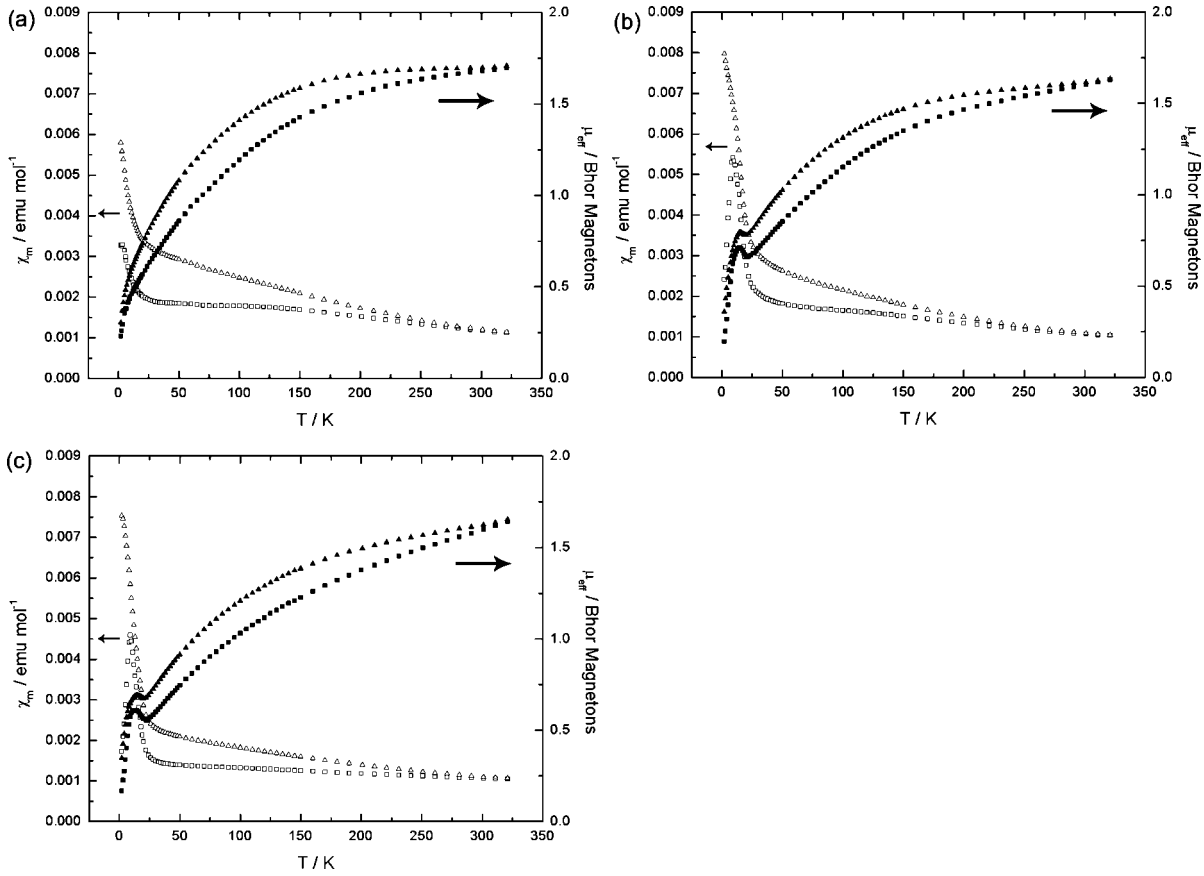

Figure 5. Molar susceptibility (open symbols) and effective magnetic moment (filled symbols) curves of (a) NiO-80, (b) NiO-100, and (c) NiO-130. The samples were measured in 0.01 T, after being cooled in both zero field (squares) and 0.01 T (triangles). Arrows on the graphs indicate the relevant axes for the data.

peaks in the four data sets confirms that the four materials possess the same basic structure (i.e., that of crystalline NiO).

Magnetization measurements were carried out on polycrystalline powder samples of mesoporous NiO with field and zero field cooling, as described in the Experimental Section. The data are presented in Figure 5, expressed both as the molar susceptibility and the effective moment ($\mu_{eff} = (8\chi_m T)^{1/2}$, where χ_m is expressed in emu mol^{-1}). The values of μ_{eff} for the mesoporous samples tend toward that of a spin ½ system (1.73 μ_B) rather than the value one would expect for a system with $S = 1$ (2.828 μ_B), as is the case in NiO.[38] The XANES experiments indicate that there is a negligible level of Ni^{3+} (which would have $S = ½$), so it is likely that our observations are intrinsic to the mesoporous NiO. Our observation of a reduced moment on Ni^{3+} compared to the value for a paramagnet at the same temperature indicates that a significant fraction freezes to some form of long-range order above the highest temperature of our measurements (bulk NiO has a Néel temperature of 523 K).[39] The remaining moments, perhaps located at sites of lower connectivity (for example, at walls or dislocations in the material), might then freeze at lower temperatures. The divergence of the fc and zfc susceptibility data from the highest temperature indicates the freezing of uncompensated moments or blocking of superparamagnetism. A more detailed understanding of the magnetic behavior observed for mesoporous NiO requires more detailed studies beyond the scope of the present paper.

Conclusion

Mesoporous NiO has been synthesized with crystalline walls and an ordered 3D pore structure, exhibiting a bimodal pore size distribution composed of small (3.3 nm) and large (11 nm) diameter pores. The presence of large pores does not depend on synthesizing a template with thick walls (an approach which has proved difficult to realize) but instead arises because one or the other of the two sets of mesopores in the template KIT-6 are filled (a large pore is composed of two walls and a pore of KIT-6). By varying the KIT-6 synthesis conditions, hence the degree of microporous bridging between the two sets of mesopores, it is possible to control the bimodal pore size distribution. More bridging leads to fewer large pores until only small pores remain. Preliminary magnetic data are compatible with a significant fraction of the moments freezing at a relatively high temperature, with further freezing on cooling. Further measurements, particularly with neutrons, are required to explore the changing character of such correlations with temperature.

Acknowledgment. P.G.B. is indebted to the EPSRC and the EU for financial support.

Supporting Information Available: Additional supporting figures. This material is available free of charge via the Internet at http://pubs.acs.org.

JA710849R

(38) Richardson, J. T.; Yiagas, D. I.; Turk, B.; Forster, K.; Twigg, M. V. *J. Appl. Phys.* **1991**, *70*, 6977.
(39) Vernon, M. W. *Phys. Status Solidi* **1970**, *37*, K1.